TWO TEMPERATURE ABLATIVE MATERIAL RESPONSE MODEL WITH APPLICATION TO LOW-DENSITY CARBON PHENOLIC ABLATORS

H. Scandelli, A. Ahmadi-Senichault, J. Lachaud

Arts et Métiers Institute of Technology, University of Bordeaux, CNRS, Bordeaux INP, INRAE, I2M Bordeaux, F-33400 Talence, France.

ABSTRACT

Ablative material response codes currently in use consider local thermal equilibrium between the solid phases and the pyrolysis gases. For typical entry conditions, this hypothesis may be justified by the fact that the thermal Peclet number within the pores is small, which is a necessary condition for thermal equilibrium in non-reactive materials. However, the validity of this analysis may fall under some circumstances. The Peclet number may become large due to high pyrolysis gas velocities. Additional physical phenomena not accounted for in the Peclet analysis may become non-negligible, such as the change of enthalpy due to chemical reactions. The objective of this study is two-fold. First, we will present a detailed two temperature material response model for porous reactive materials. This new model has been implemented and made available in the Porous material Analysis Toolbox based on OpenFOAM (PATO). Second, we will present its application to the Theoretical Ablative Composite for Open Testing (TACOT) in a wide range of conditions to assess the true range of validity of the thermal equilibrium hypothesis. Simulations are carried out on the ablation test cases $\#1$ and $\#2$, and for Stardust and for the Mars Science Laboratory atmospheric entries.

Index Terms— Local Thermal Non-Equilibrium; Thermal Protection System; TACOT; Ablation Test Cases $\#1$ $\#2$; Stardust mission; MSL mission

1. INTRODUCTION

Extra-orbital missions often involve the analysis of entry processes into planetary atmospheres at hypersonic speeds. Under these conditions, a high enthalpy curved detached shock (bow shock) forms in front of the spacecraft and the kinetic energy is progressively dissipated into heat. Convection of this flow around the capsule and radiation progressively heat the material. The temperature at the surface of the material can increase to approximately $3000\ K$ for severe entry conditions. To ensure the integrity of the structure, a thermal protection system (TPS) is designed to absorb and dissipate the heat through phase changes, chemical reactions, and material removal. Charring ablative materials represent a traditional approach to thermal protection [1, 2]. A famous example is the new class of phenolic impregnated ablators (PICA [3], PICA-X, ASTERM [4]) that consists of a carbon fiber preform partially impregnated with phenolic resin, resulting in very light weight, good insulators, and high mechanical strength. When heated, the resin thermally decomposes and progressively carbonizes, losing mass and releasing pyrolysis gases. These gases percolate and diffuse towards the surface, reacting with each other (homogeneous reactions) and with the solid phases (heterogeneous reactions). Once at the surface, the gases are blown into the flow-field boundary layer, changing its composition. The blowing also induces a blockage of the convective heat flux impinging on the surface of the spacecraft, thus reducing the thermal load. In addition, the heat shield surface is ablated due to occurrence of heterogeneous chemical reactions between the gas mixture and the surface (vaporization, sublimation, oxidation) [5].

Engineering design tools must be able to correctly predict the in-depth temperature experienced by the internal structure of the vehicle as well as the total recession of the material. As described above, an atmospheric entry involves a wide range of phenomena, which makes the development of these tools challenging. This leads to the introduction of assumptions into the design models in order to simplify the description. It is therefore important to check the accuracy of these assumptions in the assessment of the efficiency of the ablator, to avoid unnecessarily increasing the safety margin in the design process. In particular, two assumptions are considered: (1) Local Thermal Equilibrium (LTE) between the gas phase and the ablative material, meaning the gas temperature to accommodate to the solid one within the pores. It follows that, from an energy point of view, only one governing equation is enough to model the ablative material. According to Puiroux et al. [6], this assumption can generically be considered true as long as the Peclet number for heat diffusion inside the pores is small ($Pe \ll 1$). In the case of entry flow conditions, the small pore size ($d_p < 100\mu m$) and the slow pyrolysis gas flow ($v_g \sim 1$) ensure the condition to be true. However, the validity of this analysis may fall under some circumstances. The Peclet number may become large due to high pyrolysis gas velocities, or additional physical phenomena not considered in the Peclet number may turn out

to be non-negligible, such as strong change of enthalpy due to chemical reactions. Under these circumstances, a Local Thermal Non-Equilibrium (LTNE) model, i.e. two energy equations, would be necessary to accurately characterise the temperature of the gas. The importance of this aspect lies in the fact that the chemical reactions taking place in the mixture are strongly affected by the temperature of the gas. The use of LTE models, when inappropriate, may lead to an incorrect description of the gas phase. For this reason, the aim of this study is to analyse the validity of the LTE model during entry condition and to investigate possible differences with respect to a LTNE model.
(2) assumes equilibrium chemistry in the gas mixture. Although this may be acceptable for the numerical description at the surface and in the boundary layer, it is strongly believed that the assumption decays for colder mixtures within the material. A first nonequilibrium mechanism has been proposed by April and Pike, 1971 [7], after matching numerical results with experimental ones. The mechanism features 11 species and 10 chemical reactions, strongly simplifying the reality. This may lead to not satisfactory results, as already observed in the literature [8]. Due to the lack of well funded mechanism available in the literature, some authors used the reduced 22-species homogeneous finite-rate chemistry mechanism derived from the combustion database of Blanquart [9], even thought its validation has not been proved in the context of ablative materials. This work focuses on equilibrium chemistry. A second study will soon be released on the effect of LTNE model when considering non-equilibrium chemistry. The objective of this study is two-fold. First, a detailed two temperature material response model for reactive porous materials is presented. This new model has been implemented and made available in the Porous material Analysis Toolbox based on OpenFOAM (PATO). Its numerical description is presented in Section 2. Secondly, the model will be applied to the Theoretical Ablative Composite for Open Testing (TACOT) in a wide range of conditions to assess the true range of validity of the thermal equilibrium hypothesis. Simulations are carried out on the ablation test cases #1 and #2, and for Stardust and for the Mars Science Laboratory atmospheric entries. This is done in Section 3. Finally, conclusions are drawn in Section 4.

2. NUMERICAL MODEL

The material response code, PATO, has been implemented and validated over the last decade [10, 11, 12]. In what follows, a short review of its main assumptions and governing equations is presented. We invite the reader to refer to the cited articles for more details.

2.1. Main Assumption

The model provides the numerical description of the interaction between a multi-phase reactive material (N_p solid phases) with a multi-species reactive gas mixture (N_g gaseous elements/species). Any liquid phase present in the ablative material (such as water) is modelled as a solid static phase. The numerical description is carried out at the Darcy-scale (macroscopic scale). The governing equations are derived from upscaling theories [13, 14, 15], relying on the existence of a Representative Elementary Volume (REV) of the domain and on the assumption of scales separation. The specific choice of the upscaling theory is not critical, as all approaches lead to equivalent results, provided the same physical hypotheses and level of mathematical approximations [16]. In order to simplify the reading of the equations, no special notations for the averaged terms is considered in this paper. All the variables (both extensive and intensive) must to be understood as averaged terms [12].

2.2. Pyrolysis

N_p solid phases compose the material. For example, in TACOT the main components are the carbon fiber preform and the phenolic resin, which are modeled as two phases. Each solid phase, $\mathcal{P}_i$, may decompose following multiple pyrolysis kinetics. We deal with this aspect by splitting each phase i into j sub-phases. A generic sub-phase $P_{i,j}$ undergoes a determined kinetic mechanism which results in the production of species, or element, A_k according to the stoichiometric coefficients $\nu_{i,j,k}$

$$\mathcal{P}_{i,j} \longrightarrow \sum_{k=1}^{N_g} \nu_{i,j,k} A_k, \tag{1}$$

The Arrhenius model is adopted to model the pyrolysis reactions. This leads to the definition of the advancement of the pyrolysis reaction $\chi_{i,j}$ of sub-phase j within phase i as follows

$$\partial_t \chi_{i,j} = (1-\chi_{i,j})^{m_{i,j}} T_s^{n_{i,j}} \mathcal{A}_{i,j} exp\Big(-\frac{\mathcal{E}_{i,j}}{R\,T_s}\Big), \tag{2}$$

where m and n are the Arrhenius law parameters, $\mathcal{A}$ is the Arrhenius law pre-exponential factor, $\mathcal{E}$ represents the Arrhenius law activation energy, R stands for the perfect gas constant, and T_s indicates the temperature of the solid. By summing the productions of the N_p solid phases it is possible to derive the total production rate π of species/element k

$$\pi_k = \sum_{i\in[1,N_p]} \sum_{j\in[1,P_i]} \nu_{i,j,k} \epsilon_{i,0} \rho_{i,0} y_{i,j} \partial_t \chi_{i,j} \tag{3}$$

where $\epsilon_{i,0}$, $\rho_{i,0}$, and $y_{i,j}$, are respectively the initial (at t=0) volume fraction of phase i, intrinsic density of phase i, and mass fraction of sub-phase j within phase i. The overall

pyrolysis-gas production rate Π is evaluated by summing over the elements and species in the mixture

$$\Pi = \sum_{k\in[1,N_g]} \pi_k \tag{4}$$

2.3. Mass Conservation

Each solid phase, each species/element, and the gas mixture are characterized by a mass conservation equation.
For a generic solid phases i, the equation reads

$$\partial_t(\epsilon_i\rho_i) = -\pi_i - \omega_{h,i} \tag{5}$$

where ω_h represents the heterogeneous reactions contributions, t is the time, and the subscript 0 stands for the initial time ($t = 0$).
Depending on the chemistry model used in the gas phase, elements or species are considered (elements for equilibrium or species for finite-rate chemistry). In case of equilibrium chemistry, as assumed in this work, the conservation equation for a generic element with mass fraction z_k reads

$$\partial_t(\epsilon_g\rho_g z_k) + \partial_{\boldsymbol{x}} \cdot (\epsilon_g\rho_g z_k \boldsymbol{v_g}) + \partial_{\boldsymbol{x}} \cdot \boldsymbol{\mathcal{F}}_k = \pi_k \tag{6}$$

In case of finite rate chemistry, the conservation equation for a generic species with mass fraction y_i reads

$$\partial_t(\epsilon_g\rho_g y_i) + \partial_{\boldsymbol{x}} \cdot (\epsilon_g\rho_g y_i \boldsymbol{v_g}) + \partial_{\boldsymbol{x}} \cdot \boldsymbol{\mathcal{F}}_i = \pi_i + \epsilon_g\omega_i\mathcal{M}_i \tag{7}$$

where $\mathcal{M}$ is the mean molar mass of the gas mixture and $\boldsymbol{\mathcal{F}}_i$ and $\boldsymbol{\mathcal{F}}_k$ [12] are the effective multicomponent diffusion mass fluxes of the i-th species and k-th element. Mutation++ [17, 18], is used as a third party library to compute all thermodynamics and transport properties.
For the gas mixture, mass conservation accounts for the pyrolysis production rate Π and the heterogeneous reaction rate Ω_h

$$\partial_t(\epsilon_g\rho_g) + \partial_{\boldsymbol{x}} \cdot (\epsilon_g\rho_g \boldsymbol{v_g}) = -\sum_{i\in[1,N_p]} \partial_t(\epsilon_i\rho_i) = \Pi + \Omega_h \tag{8}$$

In the numerical model, a unified approach is proposed to deal with chemical reactions of solid and gas species. To model heterogeneous chemistry, solid phases are introduced into the homogeneous chemistry mechanism by modeling the effective molar density of a reacting solid phase i as

$$X_i = \frac{s_i\theta_i}{\epsilon_g} \tag{9}$$

where s_i is its specific surface and θ_i its active site density. This allows homogeneous and heterogeneous finite-rate chemistry to be solved in a coupled fashion, and effective reaction rates to be computed with improved accuracy and numerical stability.

2.4. Momentum Conservation

The average gas velocity is obtained from the resolution of Darcy's law [19]

$$\boldsymbol{v_g} = -\Big[\frac{1}{\mu}\underline{\underline{K}}\Big(1 + \frac{1}{p}\underline{\underline{\beta}}\Big)\Big] \cdot \partial_{\boldsymbol{x}} p \tag{10}$$

where p_g is the gas pressure, $\underline{\underline{K}}$ is the permeability tensor, and $\underline{\underline{b}}$ the Klinkenberg correction introduced to account for slip effects (at the pore scale) when the Knudsen number is not very small. This expression for the gas velocity vector can be substituted back into the gas mass conservation law, Eq.(8). Assuming a mixture of perfect gases, the following equation in pressure is found

$$\partial_t\Big(\frac{\epsilon_g\mathcal{M}}{RT_g}p_g\Big) - \partial_{\boldsymbol{x}} \cdot \Big[\frac{\epsilon_g\mathcal{M}}{RT_g}\frac{1}{\mu}\underline{\underline{K}}\Big(1 + \frac{1}{p_g}\underline{\underline{\beta}}\Big) \cdot \partial_{\boldsymbol{x}} p_g\Big] = \Pi + \Omega_h \tag{11}$$

where $\mathcal{M}$ and μ are the mean molar mass and the dynamic viscosity of the gas mixture.

2.5. Energy Conservation

Under the assumption of LTE, the temperature of the gas mixture accommodates to the one of the solid: $T_s = T_g = T$. A single conservation equation is then considered [12]

$$\begin{aligned}\partial_t(\rho_{tot}e_{tot}) + \partial_{\boldsymbol{x}} \cdot (\epsilon_g\rho_g h_g \boldsymbol{v}_g) = \partial_{\boldsymbol{x}} \cdot \sum_{k=1}^{N_g} \boldsymbol{Q}_k + \\ \partial_{\boldsymbol{x}} \cdot \Big(\underline{\underline{k}}_{eff} \cdot \partial_{\boldsymbol{x}} T\Big)\end{aligned} \tag{12}$$

where the subscript tot stands for total, e, h, and T denote respectively the internal energy, the absolute enthalpy, and the temperature, $\boldsymbol{Q}_k$ is the heat transport by effective diffusion of the species, and $\underline{\underline{k}}_{eff}$ represents the effective thermal conductivity tensor. The terms on the left hand-side of the equation are the ones of accumulation and advection. While, on the right hand-side there are the terms of diffusion of the pyrolysis gases and the conduction flux. The conduction flux is described by Fourier's law where the effective conductivity tensor accounts for conduction in the gas and solid phases and radiative heat transfer within the pores [11, 20].
Eq. (12) can be further developed by expressing the total storage internal energy ($\rho_{tot}\ e_{tot}$) as the sum of the energy of its phases

$$\rho_{tot}e_{tot} = \epsilon_g\rho_g e_g + \sum_{i=1}^{N_p} \epsilon_i\rho_i h_i \tag{13}$$

By substituting this term back in Eq. (12) and by performing the time derivatives, the energy conservation equation takes

its final form

$$\sum_{i=1}^{N_p} \epsilon_i \rho_i c_p \partial_t T + c_{p,g} \epsilon_g \rho_g \partial_t T = \partial_{\boldsymbol{x}} \cdot \Big(\underline{\underline{k}}_{eff} \cdot \partial_{\boldsymbol{x}} T \Big) + - \sum_{i=1}^{N_p} h_i \partial_t (\epsilon_i \rho_i) - \sum_{j=1}^{N_s} h_j \partial_t (\epsilon_g \rho_g y_j) + \partial_t (\epsilon_g p_g) + \quad (14) - \partial_{\boldsymbol{x}} \cdot (\epsilon_g \rho_g h_v \boldsymbol{v}_g) + \partial_{\boldsymbol{x}} \cdot \sum_{k=1}^{N_g} \boldsymbol{Q}_k$$

where c_p is the specific heat. All the accumulation terms are gathered on the left hand-side of the equation. Whereas, on the right hand-side it is possible to find (in order) the terms related to conduction, pyrolysis, pressure, advection, species diffusion, and viscous effects.

Under the assumption of LTNE, two energy conservation equations are needed to describe the solid and gas phases. The two equations are

$$\epsilon_s \rho_s c_{p,s} \partial_t T_s + h_s \partial_t (\epsilon_s \rho_s) = + \partial_{\boldsymbol{x}} \cdot \Big(\underline{\underline{k}}_{eff,s} \cdot \partial_{\boldsymbol{x}} T_s \Big) + + h_v \Big(T_g - T_s \Big) \quad (15)$$

and

$$\epsilon_g \rho_g c_{p,g} \partial_t T_g + \sum_{j=1}^{N_s} h_j \partial_t (\epsilon_g \rho_g y_j) - \partial_t (\epsilon_g p_g) = = - \partial_{\boldsymbol{x}} \cdot \Big(\epsilon_g \rho_g \boldsymbol{v}_g h_g \Big) + \partial_{\boldsymbol{x}} \cdot \Big(\underline{\underline{k}}_{eff,g} \cdot \partial_{\boldsymbol{x}} T_g \Big) + \quad (16) + \partial_{\boldsymbol{x}} \cdot \sum_{k=1}^{N_g} \boldsymbol{Q}_k + h_v \Big(T_s - T_g \Big)$$

where h_v is the volumetric heat transfer coefficient that identifies the heat exchanged by the two phases. It should be mentioned, if summing the two LTNE equations (Eq. (15) and Eq. (16)), the LTE equation (Eq. (14) is obtained.

3. APPLICATION OF THE MODEL TO FOUR ABLATION CASES

In this section, the numerical model is applied in order to assess the validity of the thermal equilibrium hypothesis for atmospheric entry applications. Four different ablation cases are considered: ablation test case #1 and #2, Stardust and MSL missions. A subsection is dedicated to each of them. The same ablative material, TACOT, is considered for all cases. This theoretical material is characterized by a composition and properties that are comparable to NASA's Phenolic Impregnated Carbon Ablator. In volume, TACOT is made of 10% of carbon fibers (phase-1) and 10% of phenolic resin (phase-2), hence $N_p = 2$. It is 80% porous (phase-0: gas). During the thermal degradation process, the carbon fibers phase does not decompose, while the phenolic resin undergoes several parallel pyrolysis mechanisms, as shown in Table 1. 1D Simulations have been carried out on uniform meshes. Good convergence of results has been observed when using 600 cells, at minimum. The thickness of the geometry is specified in each subsection. Equilibrium chemistry is considered in the simulations and the April mechanism [7] is considered for the composition of the gas mixture.

For each case, both the LTE (Eq. (14)) and the LTNE (Eq. (15), Eq. (16)) models are applied. Results are then compared and commented. The comparison is made in terms of temperature distribution within the material, pyrolysis gas blowing rate at the surface, wall recession due to pyrolysis ablation, and identification of the pyrolysis zone. The latter is defined as the intermediate region between two thresholds: virgin 98% and char 2%. The latter are defined as: $\rho_v(98\%) = \rho_c + 0.98(\rho_v - \rho_c)$ and $\rho_c(2\%) = \rho_c + 0.02(\rho_v - \rho_c)$. The difference between the results is quantified by their relative difference, defined as follows

$$relative\ difference = \frac{\rho_v(98\%)_{1T} - \rho_v(98\%)_{2T}}{\rho_v(98\%)_{1T}}\ 100 \quad (17)$$

where the quantity $\rho_v(98\%)$ is taken as example.

In order to apply the LTNE model, it is necessary to quantify the volumetric heat transfer coefficient between the gas phase and the TACOT material. Its value has been set equal to $h_v = 1e9\ Wm^{-3}K^{-1}$, after the study of S. Liu. More details can be found in the article submitted by Shaolin Liu for the FAR conference 2022: "Experimental investigation of heat transfer in Calcarb: one or two temperature model?".

3.1. Ablation Case #1

A sample of TACOT of 5 cm with initial conditions of $p_0 = 1\ atm$ and $T_0 = 300\ K$ is modeled. Standard air is assumed for the initial gas composition of the material. At initial time (t=0 s) the sample is heated at 1664 K for 1 minute (Dirichlet boundary condition) at atmospheric pressure, adiabatic boundary condition on the other side. When the heat flux is applied or removed, transitions of 0.1 s (linear ramping) are applied.

7 thermocouples are displaced in the material at different depth in order to provide a measure of the temperatures during the simulations. The results are shown in Fig. 1, where the position of the measurements is indicated in the legend. T_s represents both the temperature prediction from the LTE model and the solid temperature prediction from the LTNE model, as they perfectly overlap. T_g indicates the gas temperature prediction from the LTNE model. For a better understanding of the divergence between the two models, the difference $T_s - T_g$ is shown in the figure on the right. It can be appreciated that, close to the surface, the gas temperature

j	Pyrolyis of phenolic matrix	Peak (K)	$c_{2,j}$	$\mathcal{A}_{2,j}$	$\mathcal{E}_{2,j}$	$m_{2,j}$	$n_{2,j}$
1	$\mathcal{P}_{2,1} \longrightarrow H_2O$	373	0.01	$8.56 \cdot 10^3$	$7.12 \cdot 10^4$	3	0
2	$\mathcal{P}_{2,2} \longrightarrow 0.69H_2O + 0.01C_6H_6 + 0.01C_7H_8 + 0.23C_6H_6O$	773	0.24	$8.56 \cdot 10^3$	$7.12 \cdot 10^4$	3	0
3	$\mathcal{P}_{2,3} \longrightarrow 0.09CO_2 + 0.33CO + 0.58CH_4$	873	0.03	$4.98 \cdot 10^8$	$1.70 \cdot 10^5$	3	0
4	$\mathcal{P}_{2,4} \longrightarrow H_2$	1073	0.06	$4.98 \cdot 10^8$	$1.70 \cdot 10^5$	3	0

Table 1. Pyrolysis balance equations and kinetic parameters for the phenolic matrix in TACOT.

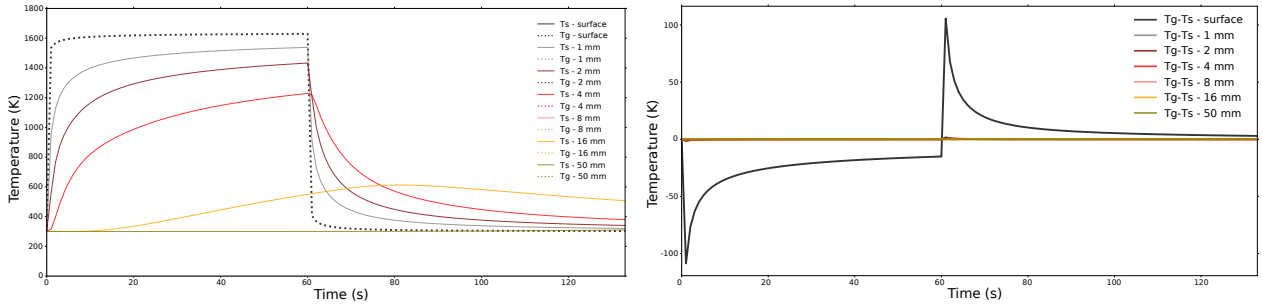

Fig. 1. Ablation test case #1. Thermocouple data are reported on the left figure and temperature difference on the right one.

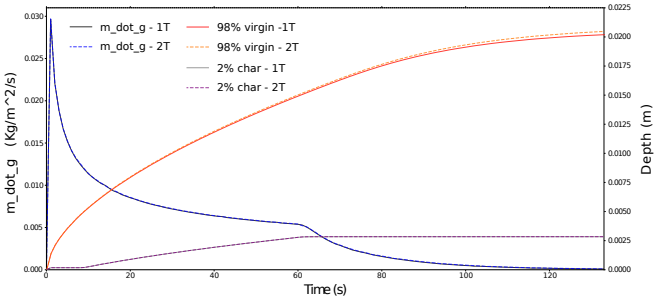

Fig. 2. Ablation test case #1. Blowing rates, pyrolysis zone, and recession.

does not match that of the solid. This means that the heat transfer coefficient is not high enough to accommodate the two temperatures at the surface when an abrupt change of condition occurs.

Comparing the temperatures behaviour within the material is not sufficient to fulfill the objective. The pyrolysis gas blowing rate at the surface, the wall recession, and the pyrolysis zone have to be considered in order to analyze the impact of the two energy models on the quantities of interest for the design process. Fig. 2 reports their evolution over time. 1T and 2T indicate that a quantity has been obtained with the LTE or LTNE model respectively. The test case #1 does not account for ablation, there is no wall recession. The figure shows how, for the blowing rate and the char threshold, the 1T and 2T predictions perfectly overlap. Using a 1T or 2T model does not affect any of these quantities. The same does not hold true for the virgin threshold, where the gas temperature causes a difference in the estimation that increases slightly with time. At the final time step, the relative error is about 1.4%.

t (s)	$\rho_e \boldsymbol{v}_e C_H$ $(Kg\ m^{-2}\ s^{-1})$	h_e $(J\ Kg^{-1})$	p_w (Pa)
0	0	0	101325
0.1	0.3	$2.5 \cdot 10^7$	101325
60	0.3	$2.5 \cdot 10^7$	101325
60.1	0	0	101325
120	0	0	101325

Table 2. Ablation test case #2. Summary of the environment properties.

3.2. Ablation Case #2

Same configuration and parameters are considered as in the ablation case #1. The only difference is in the thermal boundary condition: the Dirichlet condition is replaced by a convective condition involving the resolution of surface mass and energy balances. More information on this condition are detailed in [10]. The heat and mass transfer coefficients, as well as the surface pressure, are required as input. Data are resumed in Table 2. Earth standard environment composition are considered for the element composition at the boundary.

The same quantities are monitored and compared. The thermocouple data and the relative temperature difference are shown in Fig. 3. The gas temperature still does not adjust to that of the solid on the surface when there is a abrupt change of condition. Within the material, a one temperature description is once again valid. It can be seen that in the graph some curves are interrupted before the last time step. Ablation is the reason. The material recedes and the thermocouple stops recording the temperature value once outside the material.

The blowing rates, pyrolysis zone, and recession, are reported in Fig. 4 Once again, all the quantities are in perfect agree-

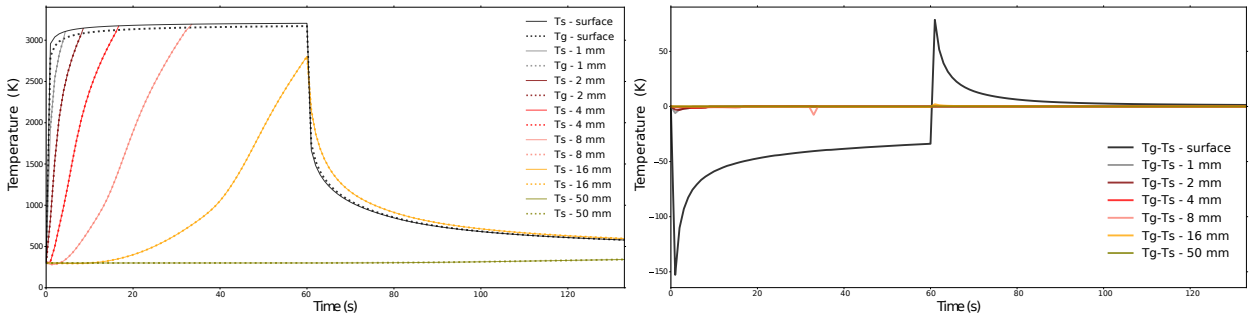

Fig. 3. Ablation test case #2. Thermocouple data are reported on the left figure and temperature difference on the right one.

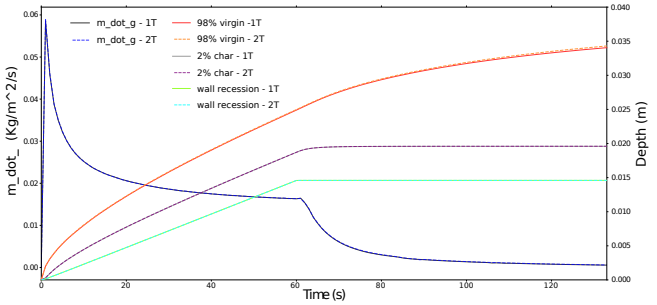

Fig. 4. Ablation test case #2. Blowing rates, pyrolysis zone, and recession.

ment, expect for the virgin characterised by a relative error of around 1%.

3.3. Stardust Ablation Case

The Stardust mission was a 390-kilogram robotic space probe launched by NASA on 7 February 1999. Its primary mission was to collect dust samples from the coma of comet Wild 2, as well as cosmic dust samples, and return these to Earth for analysis. It was the first sample-return mission of its kind. The primary mission was successfully completed on 15 January 2006, when the sample space probe returned to Earth.
The TPS is modeled as a 1D material composed of three layers: 5.8 cm of TACOT material, 0.14 cm of adhesive film (HT-424), and 1.27 cm of aluminium 2024 [21]. The convective boundary condition is adopted. An overview of the input file is given in Table 3, Earth standard environment composition are considered for the element composition at the boundary.
Results of the thermocouple and temperature difference are shown in Fig. 5 Without any abrupt change of condition, the gas temperature tends to be closer to that of the solid. Referring to the figure on the right, it can be seen that at most, the difference between the two predictions is about 25 K. Considering that the temperatures are about 3000 K, the 25 K difference can be considered negligible. In fact, in the figure on the left, the temperature curves of the gas and the solid are superimposed at each position. This aspect is also reflected in the

t (s)	p_w (Pa)	C_m $(Kg/m^2/s)$	h_w (J/Kg)
0	1.5	0.00005	77926960
1	1.8	0.00006	77984280
2	2.1	0.00007	78040736
3	2.4	0.00008	78095240
4	2.6	0.00009	78146168
..	..	..	..
50	19142.319	0.17378	61280148
51	21350.19075	0.18082	59093460
52	23558.0625	0.18786	56748968
..	..	..	..
131	2144.746275	0.01705	95178
132	2067.8406	0.01644	89990
133	2067.8406	0.01582	84957

Table 3. Stardust case. Partial summary of the environment properties.

comparison of the quantities of interest. This is represented in Fig. 6, where the maximum relative difference, 0.2% is related to the prediction of the location of the virgin front.

3.4. MSL Ablation Case

The Mars Science Laboratory (MSL) mission was a robotic space probe mission to Mars launched by NASA on November 26, 2011. It successfully landed Curiosity, a Mars rover, in Gale Crater on August 6, 2012. The overall objectives include investigating Mars' habitability, studying its climate and geology, and collecting data for a human mission to Mars.
The depth of the ablative material is now of 4.385 cm [22]. The Mars atmosphere is considered for the initial gas composition of the material and for the composition of the element in the boundary layer. The input data for the convective boundary layer are taken from the study by Meurisse et al., 2018 [22]. The thermocouple and temperature difference results are shown in Fig. 7. A difference of 40 K is reached at the beginning of the simulation between the two temperatures due to the initial sharp change of condition. After this initial time, the error decreases slightly with time. Nevertheless, as

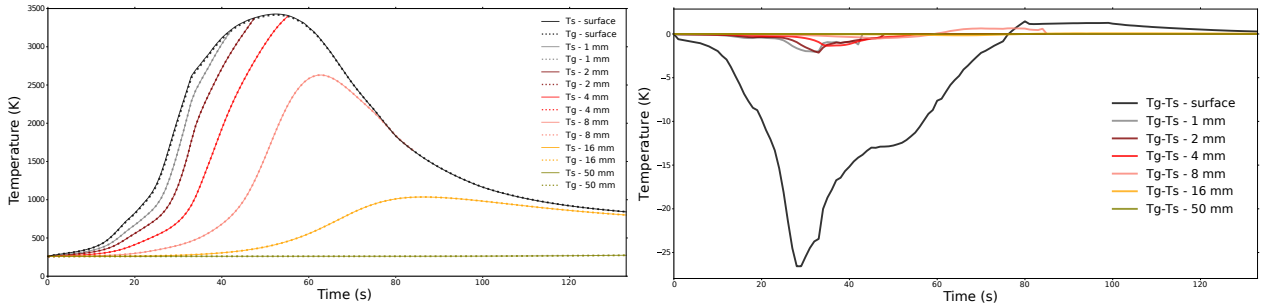

Fig. 5. Stardust case. Thermocouple data are reported on the left figure and temperature difference on the right one.

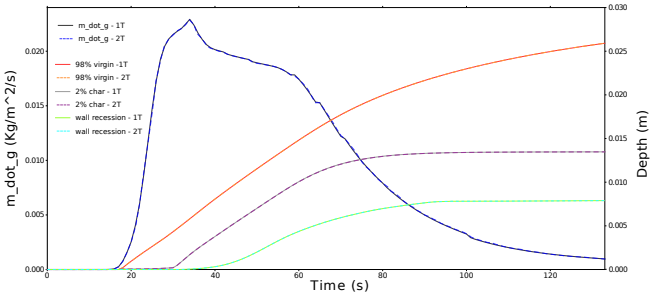

Fig. 6. Stardust case. Blowing rates, pyrolysis zone, and recession.

can be seen in Fig. 8, this small difference in temperature does not lead to any discrepancy on any quantities of interest. The maximum relative error is still provided by the prediction of the virgin front location. Its value is only 0.2%.

4. CONCLUSIONS

This study investigates the validity of the local thermal equilibrium assumption for ablative material response codes. To this end, a two-temperature model has been implemented and integrated in the Porous material Analysis Toolbox based on OpenFOAM (PATO). This toolbox has been then applied to the Theoretical Ablative Composite for Open Testing (TACOT) in a wide range of conditions to assess the true range of validity of the thermal equilibrium hypothesis. 1D simulations are performed on the ablation test cases $\#1$ and $\#2$, as well as on the Stardust and Mars Science Laboratory atmospheric entry missions. Both Local Thermal Equilibrium (LTE) and Local Thermal Non-Equilibrium (LTNE) energy models have been adopted. The comparison between the two models has been carried out by monitoring the evolution of the temperature inside the material, the pyrolysis gas blowing rate, the pyrolysis zone, and the wall recession due to ablation. Results show how the gas temperature does not match perfectly that of the solid on at the surface, especially when a sudden change in conditions occurs. Nevertheless, the temperature difference does not lead to a significant deviation in the monitored quantities (the maximum relative difference in the results has been found to be about 1.4%). The relative difference values are possible source of uncertainty to include in design analysis. All simulations assume equilibrium chemistry. The analysis in the case of non-equilibrium chemistry will be conducted in a future work. Preliminary analysis show a large impact due to the enthalpies of reactions.

5. ACKNOWLEDGMENTS

The research of H.S. was sponsored by a PhD grant awarded by Arts et Métiers Institute of Technology.

6. REFERENCES

[1] Michael J Wright, Robin AS Beck, Karl T Edquist, David Driver, Steven A Sepka, Eric M Slimko, and William H Willcockson, "Sizing and margins assessment of mars science laboratory aeroshell thermal protection system," *Journal of Spacecraft and Rockets*, vol. 51, no. 4, pp. 1125–1138, 2014.

[2] Mairead Stackpoole, Steve Sepka, Ioana Cozmuta, and Dean Kontinos, "Post-flight evaluation of stardust sample return capsule forebody heatshield material," in *46th AIAA Aerospace Sciences Meeting and Exhibit*, 2008, p. 1202.

[3] Huy K Tran, C Johnson, D Rasky, F Hui, Ming-Ta Hsu, Timothy Chen, Y Chen, Daniel Paragas, and Loreen Kobayashi, "Phenolic impregnated carbon ablators pica as thermal protection system for discovery missions," *NASA TM-110440, NASA, Washington, DC*, 1997.

[4] H Ritter, P Portela, K Keller, JM Bouilly, and S Burnage, "Development of a european ablative material for heatshields of sample return missions," in *6th European Workshop on Thermal Protection Systems and Hot Structures, Stuttgart, Germany*, 2009, vol. 99.

[5] Alexandre Martin and Iain D Boyd, "Modeling of heat transfer attenuation by ablative gases during the stardust

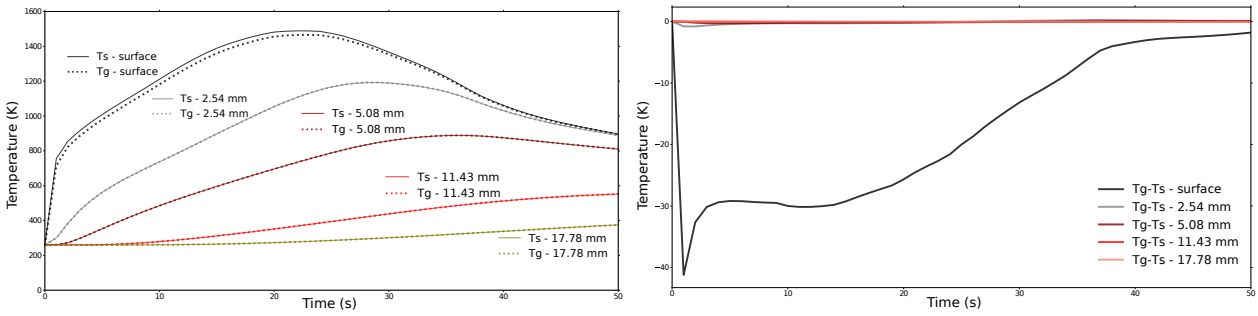

Fig. 7. MSL case. Thermocouple data are reported on the left figure and temperature difference on the right one.

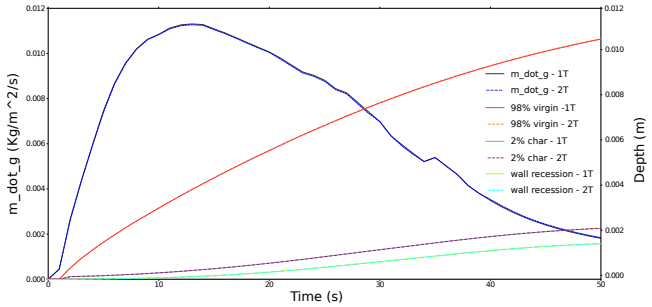

Fig. 8. MSL case. Blowing rates, pyrolysis zone, and recession.

reentry," *Journal of Thermophysics and Heat Transfer*, vol. 29, no. 3, pp. 450–466, 2015.

[6] N Puiroux, Marc Prat, and Michel Quintard, "Non-equilibrium theories for macroscale heat transfer: ablative composite layer systems," *International Journal of Thermal Sciences*, vol. 43, no. 6, pp. 541–554, 2004.

[7] Gary C April, Ralph W Pike, and EDUARDO G DEL VALLE, "Modeling reacting gas flow in the char layer of an ablator," *AIAA Journal*, vol. 9, no. 6, pp. 1113–1119, 1971.

[8] Balaji Shankar Venkatachari, Gary Cheng, Roy Koomullil, and Anahita Ayasoufi, "Computational tools for re-entry aerothermodynamics: Part ii. surface ablation," in *46th AIAA Aerospace Sciences Meeting and Exhibit*, 2008, p. 1218.

[9] G Blanquart, P Pepiot-Desjardins, and H Pitsch, "Chemical mechanism for high temperature combustion of engine relevant fuels with emphasis on soot precursors," *Combustion and Flame*, vol. 156, no. 3, pp. 588–607, 2009.

[10] Jean Lachaud and Nagi N Mansour, "Porous-material analysis toolbox based on openfoam and applications," *Journal of Thermophysics and Heat Transfer*, vol. 28, no. 2, pp. 191–202, 2014.

[11] Jean Lachaud, Tom van Eekelen, James B Scoggins, Thierry E Magin, and Nagi N Mansour, "Detailed chemical equilibrium model for porous ablative materials," *International Journal of Heat and Mass Transfer*, vol. 90, pp. 1034–1045, 2015.

[12] Jean Lachaud, James B Scoggins, Thierry E Magin, MG Meyer, and Nagi N Mansour, "A generic local thermal equilibrium model for porous reactive materials submitted to high temperatures," *International Journal of Heat and Mass Transfer*, vol. 108, pp. 1406–1417, 2017.

[13] Gedeon Dagan and Shlomo P Neuman, *Subsurface flow and transport*, International Hydrology Series, 1997.

[14] Stephen Whitaker, *The method of volume averaging*, vol. 13, Springer Science & Business Media, 2013.

[15] E Sanchez-Palencia, "Homogenization method for the study of composite media," in *Asymptotic Analysis II—*, pp. 192–214. Springer, 1983.

[16] John H Cushman, Lynn S Bennethum, and Bill X Hu, "A primer on upscaling tools for porous media," *Advances in Water Resources*, vol. 25, no. 8-12, pp. 1043–1067, 2002.

[17] James B Scoggins and Thierry E Magin, "Development of mutation++: Multicomponent thermodynamic and transport properties for ionized plasmas written in c++," in *11th AIAA/ASME joint thermophysics and heat transfer conference*, 2014, p. 2966.

[18] James B Scoggins and Thierry E Magin, "Gibbs function continuation for linearly constrained multiphase equilibria," *Combustion and Flame*, vol. 162, no. 12, pp. 4514–4522, 2015.

[19] Stephen Whitaker, "Flow in porous media i: A theoretical derivation of darcy's law," *Transport in porous media*, vol. 1, no. 1, pp. 3–25, 1986.

[20] AJ Van Eekelen and J Lachaud, "Numerical validation of an effective radiation heat transfer model for fiber preforms," *Journal of Spacecraft and Rockets*, vol. 48, no. 3, pp. 534–537, 2011.

[21] Kerry A Trumble, Ioana Cozmuta, Steve Sepka, Peter Jenniskens, and Michael Winter, "Postflight aerothermal analysis of the stardust sample return capsule," *Journal of Spacecraft and Rockets*, vol. 47, no. 5, pp. 765–774, 2010.

[22] Jeremie BE Meurisse, Jean Lachaud, Francesco Panerai, Chun Tang, and Nagi N Mansour, "Multidimensional material response simulations of a full-scale tiled ablative heatshield," *Aerospace Science and Technology*, vol. 76, pp. 497–511, 2018.